# Asymmetric simple exclusion process on chains with a shortcut

Nadezhda Bunzarova,[1,2] Nina Pesheva,[2] and Jordan Brankov[1,2]
[1]*Bogoliubov Laboratory of Theoretical Physics, Joint Institute for Nuclear Research, 141980 Dubna, Russian Federation*
[2]*Institute of Mechanics, Bulgarian Academy of Sciences, 1113 Sofia, Bulgaria*
(Received 2 December 2013; published 21 March 2014)

We consider the asymmetric simple exclusion process (TASEP) on an open network consisting of three consecutively coupled macroscopic chain segments with a shortcut between the tail of the first segment and the head of the third one. The model was introduced by Y.-M. Yuan *et al.* [J. Phys. A **40**, 12351 (2007)] to describe directed motion of molecular motors along twisted filaments. We report here unexpected results which revise the previous findings in the case of maximum current through the network. Our theoretical analysis, based on the effective rates' approximation, shows that the second (shunted) segment can exist in both low- and high-density phases, as well as in the coexistence (shock) phase. Numerical simulations demonstrate that the last option takes place in finite-size networks with head and tail chains of equal length, provided the injection and ejection rates at their external ends are equal and greater than one-half. Then the local density distribution and the nearest-neighbor correlations in the middle chain correspond to a shock phase with completely delocalized domain wall. Upon moving the shortcut to the head or tail of the network, the density profile takes a shape typical of a high- or low-density phase, respectively. Surprisingly, the main quantitative parameters of that shock phase are governed by a positive root of a cubic equation, the coefficients of which linearly depend on the probability of choosing the shortcut. Alternatively, they can be expressed in a universal way through the shortcut current. The unexpected conclusion is that a shortcut in the bulk of a single lane may create traffic jams.

DOI: 10.1103/PhysRevE.89.032125 PACS number(s): 05.40.−a, 02.50.Ey, 05.60.−k, 05.70.Ln

## I. INTRODUCTION

The asymmetric simple exclusion process (TASEP) is one of the paradigmatic models for understanding the rich world of nonequilibrium phenomena. Devised to model kinetics of protein synthesis [1], it has found a number of applications for vehicular traffic flow [2], biological transport [3], one-dimensional surface growth [4], forced motion of colloids in narrow channels [5], spintronics [6], transport of "data packets" on the Internet [7], and current through chains of quantum dots [8], to mention a few.

Novel features of the TASEP have been found on networks consisting of coupled linear chains with nontrivial geometry. In the approach advanced in our work [9] each macroscopic segment $s$ of the network is considered in a stationary phase determined by its effective injection $\alpha_s^*$ and ejection $\beta_s^*$ rates. Exact in the thermodynamic limit results for the density profile are incorporated. The only molecular-field-type approximation used consists in the neglect of correlations between different chain segments. This allows one to treat the coupling between each two connected segments as coupling to reservoirs with certain effective rates. The possible phase structures of the whole network are obtained as solutions of the resulting set of equations for the effective rates that follow from the continuity of current. The importance of our approach for modeling complex biological transport phenomena was pointed out by Pronina and Kolomeisky [10]. This method became very popular and was used in a number of studies of TASEP and its generalizations on networks with, e.g., junctions, bifurcations, intersections, interacting lanes [11]. Finite-size effects on the density profile due to shifting the position of the double-chain section from the middle of an open network were studied too [12].

Here we consider the TASEP on an open chain with a shortcut in the bulk, introduced as "model A" in Ref. [13]. The current through the shortcut is proportional to a probability $q$. It is convenient to consider the system as composed of three consecutively connected macroscopic chain segments and a shortcut between the tail of the first segment and the head of the third one; see Fig. 1.

In principle, the effect of a shortcut can easily be understood: the decrease in the current through the shunted part (second segment) of the original chain leads to a sharp change of the particle density in the latter. If the chain without a shortcut ($q = 0$) is in the low-density ($\mathcal{L}$) phase, its bulk density $\rho_{\rm bulk}^{\mathcal{L}} < 1/2$ supports a current $J < 1/4$. The shortcut takes a part $J^{\rm sc} > 0$ of that current away from the second segment, hence the current $J^{(2)} = J - J^{\rm sc}$ has to be supported by still less bulk density $\rho_{\rm bulk}^{(2)} < \rho_{\rm bulk}^{\mathcal{L}}$ in that segment. Similarly, when the initial chain is in the high-density ($\mathcal{H}$) phase with $\rho_{\rm bulk}^{\mathcal{H}} > 1/2$, the drop in the current through the second segment leads to a still higher bulk density in that segment, $\rho_{\rm bulk}^{(2)} > \rho_{\rm bulk}^{\mathcal{H}}$. Not so simple is the situation when the initial chain is in the maximum current ($\mathcal{M}$) phase with $\rho_{\rm bulk}^{\mathcal{M}} = 1/2$. Now the drop in the current through the shunted segment of the network can be compensated equally well by a decrease or increase in its bulk density. Then the middle segment is forced either in the $\mathcal{L}$ or in the $\mathcal{H}$ phase, which may also lead to coexistence of the $\mathcal{L}$ phase on the left-hand side with the $\mathcal{H}$ phase on the right-hand side. This phase structure is additionally favored by the downward (upward) bend in the density profile of the first (third) segment in the maximum current phase. In the case of an open system the coexisting phases are likely to be separated by a completely delocalized domain wall. Such was the situation observed in each of the equivalent segments in a double-chain section incorporated in the middle of a long chain carrying a maximum current [9]. It seems plausible that the above mechanism of influence of the shortcut on the phase state of the shunted segment should

 

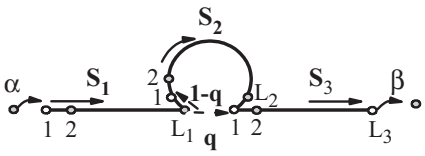


FIG. 1. Schematic representation of the network geometry. The three segments are denoted by $S_k$, $k = 1,2,3$. The shortcut is shown by a dashed arrow.

be invariant with respect to its explicit structure. In particular, one may consider a shortcut in the form of an additional chain connecting the last site of the first segment to the first site of the third one. Since the length of the shortcut is irrelevant, we can include the case of parallel segments with equal length considered in our work [9]. However, the authors of Ref. [13] have claimed that in the case of a maximum current, the shunted middle segment of their "model A" can exist only in the high-density phase. This contrast in the conclusions motivated us to renew the study, both analytically and numerically, of the model. The results may have important implications for vehicular traffic flow control, as well as for biological transport in living cells.

## II. MICROSCOPIC MODEL

Here we consider "model A" of a shortcut, proposed in Ref. [13], when both the injection $\alpha$ and ejection $\beta$ rates at the open ends of the system are larger than $1/2$, so that the first and third segments are in the maximum current phase. Let $\tau_i^{(s)}$ be the occupation number of site $i = 1,2,\ldots,L_s$ of the segment $s = 1,2,3$. According the rules of the random-sequential algorithm, when a particle at the last site of the first segment (with $\tau_L^{(1)} = 1$) attempts to move, it may jump along the main track to the first site of the second segment with rate $(1-q)(1-\tau_1^{(2)})(1-\tau_1^{(3)}) + (1-\tau_1^{(2)})\tau_1^{(3)}$, or take the shortcut to the first site of the third segment with rate $q(1-\tau_1^{(3)})$, or stay immobile with rate $(1-q)\tau_1^{(2)}(1-\tau_1^{(3)}) + \tau_1^{(2)}\tau_1^{(3)}$. These rules lead to the following exact expressions for the stationary current through the second segment:

$$J^{(2)} = (1-q)\langle\tau_L^{(1)}\big(1-\tau_1^{(2)}\big)\big(1-\tau_1^{(3)}\big)\rangle + \langle\tau_L^{(1)}\big(1-\tau_1^{(2)}\big)\tau_1^{(3)}\rangle, \quad (1)$$

where $0 \leqslant q \leqslant 1$, and through the shortcut,

$$J^{\rm sc} = q\langle\tau_L^{(1)}\big(1-\tau_1^{(3)}\big)\rangle, \quad 0 \leqslant q \leqslant 1. \quad (2)$$

In addition to (1), we have

$$J^{(2)} = \langle\tau_L^{(2)}\big(1-\tau_1^{(3)}\big)\rangle. \quad (3)$$

The vehicular interpretation of the model is obvious. The driver chooses the shortcut with a fixed probability $q$, independently of the fact whether the main road (segment 2) is open ($\tau_1^{(2)} = 0$) or not ($\tau_1^{(2)} = 1$). If the shortcut is closed ($\tau_1^{(3)} = 1$) and the main road open ($\tau_1^{(2)} = 0$), then the vehicle proceeds to the latter with rate 1. However, according to Ref. [13] vehicular traffic is better described by their "model B" in which there are two types of drivers (particles), say, the type 1 drivers are aware of the shortcut, and the type 2 ones are not. If the first site of the network is empty, particles are injected with rate $\alpha$, so that the particle is of type 1 with probability $q$, and of type 2 with probability $1-q$. Particles of type 1 (type 2) will always (never) use the shortcut.

In a biological context, the shortcut is designed to model the situation when the filament, along which the molecular motor is moving step by step, is twisted so that two sites $i$ and $j$ which are distant along the chain become close in space, thus giving a chance for the motor to jump directly from site $i$ to $j$.

## III. THEORETICAL ANALYSIS

In the effective rates analysis [9] one neglects the correlations between sites belonging to different segments, so that the above expressions simplify to

$$J^{(2)} = \rho_L^{(1)}\big(1-\rho_1^{(2)}\big)\big[(1-q)\big(1-\rho_1^{(3)}\big)+\rho_1^{(3)}\big] = \rho_L^{(2)}\big(1-\rho_1^{(3)}\big), \quad (4)$$

and $J^{\rm sc} = q\rho_L^{(1)}(1-\rho_1^{(3)})$, where $\rho_i^{(s)} = \langle\tau_i^{(s)}\rangle$, s = 1,2,3, is the average value of the occupation number $\tau_i^{(s)}$ in a given stationary state. Within the above approximation effective injection, $\alpha_s^*$, and ejection, $\beta_s^*$, rates for segment $s = 1,2,3$ are introduced according to the rule $J^{(s)} = \beta_s^*\rho_L^{(s)} = \alpha_s^*(1-\rho_1^{(s)})$, with $\alpha_1^* = \alpha$ and $\beta_3^* = \beta$ [9]. Since $J^{(1)} = J^{(3)} = J^{(2)} + J^{\rm sc}$, one obtains

$$\alpha_1^* = \alpha, \quad \beta_1^* = 1-\rho_1^{(2)} + q\rho_1^{(2)}\big(1-\rho_1^{(3)}\big), \quad (5)$$

$$\alpha_2^* = \rho_L^{(1)}\big[1-q\big(1-\rho_1^{(3)}\big)\big], \quad \beta_2^* = 1-\rho_1^{(3)}, \quad (6)$$

$$\alpha_3^* = \rho_L^{(2)} + q\rho_L^{(1)}, \quad \beta_3^* = \beta. \quad (7)$$

Expressions (5)–(7) for the effective rates coincide exactly with Eqs. (4) obtained in Ref. [13]. However, the results of our analysis are essentially different from those claimed in Ref. [13].

We study the possible phase structures of the type ($\mathcal{M}$, $\mathcal{X}$, $\mathcal{M}$), when the first and third segments are in the maximum current phase ($\mathcal{M}$), and the second segment is in a low-density phase ($\mathcal{X} = \mathcal{L}$), high-density one ($\mathcal{X} = \mathcal{H}$), or on the coexistence line ($\mathcal{X} = \mathcal{C}$). The case $\mathcal{X} = \mathcal{M}$ is excluded, since the presence of a shortcut implies $J^{(2)} < J^{(1)} = J^{(3)} = 1/4$. To check the consistency of a given structure with the corresponding conditions on the effective rates (5)–(7), we make use of the known, exact in the thermodynamic limit, values of the bulk density $\rho_{\rm bulk}^{(s)}$ and local densities $\rho_1^{(s)}$, $\rho_L^{(s)}$, in dependence on the thermodynamic phase of each segment [14]. For simplicity, in our computer simulations we assume that all the segments have an equal, large enough length $L \gg 1$. Thus, in all cases under consideration $\rho_{\rm bulk}^{(1)} = \rho_{\rm bulk}^{(3)} = 1/2$, and

$$\rho_1^{(1)} = 1 - 1/(4\alpha), \quad \rho_L^{(1)} = 1/(4\beta_1^*), \quad (8)$$

$$\rho_1^{(3)} = 1 - 1/(4\alpha_3^*), \quad \rho_L^{(3)} = 1/(4\beta). \quad (9)$$

By inserting the expressions for $\rho_L^{(1)}$ and $\rho_1^{(3)}$ into Eq. (6), we obtain

$$\alpha_2^* = 1/(4\beta_1^*) - q/(16\alpha_3^*\beta_1^*), \quad \beta_2^* = 1/(4\alpha_3^*), \quad (10)$$

and, from Eq. (4), $J^{\rm sc} = 1/4 - J^{(2)} = q/(16\beta_1^*\alpha_3^*)$.

The challenge of the problem to be solved rests in the self-adaptive feature of the local density profiles in the interior of the network. Indeed, for a fixed network, the external rates $\alpha,\beta > 1/2$ are only under control, which uniquely determine the bulk densities of the first and third segment, as well as the local densities at the external ends of the network, $\rho_1^{(1)}$ and $\rho_L^{(3)}$; see Eqs. (8) and (9). Therefore, observing these quantities only, one cannot tell whether there is some network (a "black box") in the interior, or one deals with a simple chain in the maximum current phase. In our case, the phase of the middle segment depends on the values of its effective injection and ejection rates, $\alpha_2^*$ and $\beta_2^*$, respectively, which couple to the other two internal rates $\beta_1^*$ and $\alpha_3^*$ via Eqs. (10). The latter rates, $\beta_1^*$ and $\alpha_3^*$, are related, in turn, to the local densities at the last site of the first segment and the first site of the third segment. Moreover, given the value of the shortcut parameter $q$, they determine the currents through the shortcut, $J^{\rm sc}$, and through the second segment, $J^{(2)} = 1/4 - J^{\rm sc}$. However, the current $J^{(2)}$ has to be supported by the bulk density $\rho_{\rm bulk}^{(2)}$ of the second segment, which equals $\alpha_2^*$ in the low-density phase and $1-\beta_2^*$ in the high-density one; see Eqs. (11) and (18) below. Since the current $J^{(2)}$ depends on the phase of the second segment, for each option one has to solve a closed set of equations for the four effective rates. If these equations have a solution such that $\alpha_2^* < \beta_2^* < 1/2$ ($\beta_2^* < \alpha_2^* < 1/2$), then the middle segment will be in the low- (high-) density phase. If $\alpha_2^* = \beta_2^* < 1/2$ happens to be a solution too, then the coexistence phase takes place. Thus, the internal state of the network is a result of self-adaptive changes in the shape of the local density profiles which are constrained by the current conservation at each vertex.

Now we pass to the separate consideration of each of the possibilities $\mathcal{X} = \mathcal{L}, \mathcal{H}, \mathcal{C}$.

### A. Middle segment in the low-density phase

In this case we have the following exact in the thermodynamic limit expressions:

$$\begin{aligned} &\rho_{\rm bulk}^{(2)} = \rho_1^{(2)} = \alpha_2^*, \quad J^{(2)} = \alpha_2^*(1-\alpha_2^*), \\ &\rho_L^{(2)} = \alpha_2^*(1-\alpha_2^*)/\beta_2^*. \end{aligned} \tag{11}$$

Substituting the expressions for $\rho_1^{(2)}$ and $\rho_L^{(2)}$ into Eqs. (5) and (7), we find

$$\begin{aligned} &\beta_1^* = 1 - \alpha_2^*[1 - q/(4\alpha_3^*)], \\ &\alpha_3^* = \alpha_2^*(1-\alpha_2^*)/\beta_2^* + q/(4\beta_1^*). \end{aligned} \tag{12}$$

We have obtained a set of four nonlinear equations, (10) and (12), for the four effective rates $\beta_1^*$, $\alpha_2^*$, $\beta_2^*$, and $\alpha_3^*$. From Eqs. (10) and the first equation in (12) we obtain

$$\beta_1^* = 1/[1 + 4(\alpha_2^*)^2], \tag{13}$$

$$\alpha_3^* = q[1 + 4(\alpha_2^*)^2]/[4(1-2\alpha_2^*)^2], \tag{14}$$

$$\beta_2^* = (1-2\alpha_2^*)^2/\{q[1 + 4(\alpha_2^*)^2]\}. \tag{15}$$

The above expressions for $\beta_1^*$, $\alpha_3^*$ and $\beta_2^*$ identically satisfy the second equation in (12) with respect to $\alpha_2^* = \rho_1^{(2)}$. The $(\mathcal{M},\mathcal{L},\mathcal{M})$ phase structure of the network requires $\alpha_2^* < 1/2$. Then $\beta_1^* > 1/2$, which, together with $\alpha > 1/2$, ensures that the first segment is in the $\mathcal{M}$ phase. The condition $\alpha_2^* < \beta_2^*$ for the second segment to be in the $\mathcal{L}$ phase leads to the cubic inequality

$$4q(\alpha_2^*)^3 - 4(\alpha_2^*)^2 + (4+q)\alpha_2^* - 1 < 0. \tag{16}$$

This inequality has to be fulfilled simultaneously with the condition $\alpha_3^* > 1/2$ for the third segment to be in the $\mathcal{M}$ phase (given $\beta > 1/2$). Therefore, the free parameter $\alpha_2^*$ has to obey the constraints

$$q\alpha_2^*[1 + 4(\alpha_2^*)^2] < (1-2\alpha_2^*)^2 < (q/2)[1 + 4(\alpha_2^*)^2]. \tag{17}$$

As a simple consequence, in the case of $q \to 0^-$ the free parameter $\alpha_2^* \to 1/2^-$, which agrees with the result $\alpha_2^* = \rho_{\rm bulk} = 1/2$ for a single chain in the maximum current phase.

### B. Middle segment in the high-density phase

In this case the exact thermodynamic parameters of the second segment are

$$\begin{aligned} &\rho_{\rm bulk}^{(2)} = \rho_L^{(2)} = 1 - \beta_2^*, \quad J^{(2)} = \beta_2^*(1-\beta_2^*), \\ &\rho_1^{(2)} = 1 - \beta_2^*(1-\beta_2^*)/\alpha_2^*. \end{aligned} \tag{18}$$

Substituting the above expressions for $\rho_1^{(2)}$ and $\rho_L^{(2)}$ into Eqs. (5) and (7), we find

$$\begin{aligned} &\beta_1^* = q/(4\alpha_3^*) + [1 - q/(4\alpha_3^*)]\beta_2^*(1-\beta_2^*)/\alpha_2^*, \\ &\alpha_3^* = 1 - \beta_2^* + q/(4\beta_1^*). \end{aligned} \tag{19}$$

Taking into account Eqs. (10), we have again a set of four nonlinear equations for the four effective rates. From Eqs. (10) and the second equation in (19) we obtain

$$\alpha_3^* = 1/(4\beta_2^*), \tag{20}$$

$$\beta_1^* = q\beta_2^*/[1 - 4\beta_2^*(1-\beta_2^*)], \tag{21}$$

$$\alpha_2^* = [1/(q\beta_2^*) - 1][1/4 - \beta_2^*(1-\beta_2^*)]. \tag{22}$$

The above expressions for $\alpha_2^*$, $\alpha_3^*$, and $\beta_1^*$ satisfy the first equation in (19) identically with respect to $\beta_2^* = 1 - \rho_L^{(2)}$. The phase structure $(\mathcal{M},\mathcal{H},\mathcal{M})$ requires $\alpha_2^* > \beta_2^*$, which leads to the cubic inequality

$$4q(\beta_2^*)^3 - 4(\beta_2^*)^2 + (4+q)\beta_2^* - 1 > 0. \tag{23}$$

Together with $\beta_2^* < 1/2$ it ensures the second segment to be in the $\mathcal{H}$ phase. The first segment is in the $\mathcal{M}$ phase when $\alpha > 1/2$ and $\beta_1^* > 1/2$. The second condition leads to the inequality

$$q\beta_2^* > (1/2)[1 - 4\beta_2^*(1-\beta_2^*)].$$

Hence, $q \to 0^+$ implies $\beta_2^* \to 1/2^-$, hence $J^{(2)} \to 1/4^-$ and $J^{\rm sc} \to 0^+$. The condition $\alpha_3^* > 1/2$ for the third segment to be in the $\mathcal{M}$ phase (given $\beta > 1/2$) is satisfied whenever $\beta_2^* < 1/2$.

### C. Middle segment on the coexistence line

The second segment can exist in a $\mathcal{L}$ or $\mathcal{H}$ phase, depending on whether $\alpha_2^* > \beta_2^*$ or $\alpha_2^* < \beta_2^*$, respectively. Naturally, we expect the coexistence phase $\mathcal{C}$ to take place at a common point in the closure of the above open sets, i.e., when the rates $\alpha_2^* = \beta_2^*$ coincide with an appropriate root of the cubic equation given by an equality sign in expressions (23) and (16). To prove this, we set $\alpha_2^* = \beta_2^*$ and assume the exact in the thermodynamic limit values

$$J^{(2)} = \alpha_2^*(1-\alpha_2^*), \tag{24}$$

$$\rho_1^{(2)} = \alpha_2^* = \rho_-^{(2)}, \tag{25}$$

$$\rho_L^{(2)} = 1-\alpha_2^* = \rho_+^{(2)}. \tag{26}$$

Here $\rho_\mp^{(2)} = \rho_\mp(J^{(2)})$ with $\rho_\pm(J) = (1 \pm \sqrt{1-4J})/2$ are the bulk densities in the $\mathcal{L}$ and $\mathcal{H}$ phases, respectively. Substituting the above expressions for $\rho_1^{(2)}$ and $\rho_L^{(2)}$ into Eqs. (5) and (7), we obtain

$$\beta_1^* = \rho_+^{(2)} + q\rho_+^{(2)}/(4\alpha_3^*), \tag{27}$$

$$\alpha_3^* = \rho_+^{(2)} + q/(4\beta_1^*). \tag{28}$$

Inserting in the first equation $1/(4\alpha_3^*)$ expressed from the second equation in (10) with $\beta_2^* = \alpha_2^*$, and replacing $\rho_+^{(2)}$ and $\rho_-^{(2)}$ by $1-\alpha_2^*$ and $\alpha_2^*$, respectively, we obtain

$$\beta_1^* = 1-\alpha_2^* + q(\alpha_2^*)^2. \tag{29}$$

On the other hand, dividing both sides of the first equation in (28) by $4\beta_1^*$, and using $J^{\rm sc} = 1/4 - J^{(2)}$, we arrive at

$$1/4 = \rho_+^{(2)}/(4\beta_1^*) + \rho_-^{(2)}\left(1/4 - J^{(2)}\right). \tag{30}$$

Solving the above equation for $\beta_1^*$ we obtain

$$\beta_1^* = [1+4(\alpha_2^*)^2]^{-1}. \tag{31}$$

Clearly, $\beta_1^* > 1/2$ when $\alpha_2^* < 1/2$. The equality on the right-hand sides of the two above derived expressions for $\beta_1^*$ leads to the cubic equation

$$4q(\alpha_2^*)^3 - 4(\alpha_2^*)^2 + (4+q)\alpha_2^* - 1 = 0. \tag{32}$$

Unexpectedly, the value of $\alpha_2^* = \beta_2^*$ is determined as a function of $q$, $0 \leqslant q \leqslant 1$, by the real root of Eq. (32), which is less than $1/2$ and tends to $1/2^-$ as $q \to 0^+$. A comparison of the values of $\alpha_2^*$ given by this root of (32) and $\rho_1^{(2)}$, evaluated by computer simulations, is shown in Fig. 2. From the second equation in (10) at $\beta_2^* = \alpha_2^*$ we have $\alpha_3^* = 1/(4\alpha_2^*)$, so that $\alpha_2^* < 1/2$ directly implies $\alpha_3^* > 1/2$.

### D. Predictions of the domain wall theory

An open chain with stationary current $J < 1/4$ can be found in low-density $\rho_-(J)$ and high-density $\rho_+(J)$ phases. According to the domain wall theory [15], on the coexistence line these phases are separated by a completely delocalized domain wall. As a result, the averaged density profile is linearly increasing from $\rho_-(J)$ at the left end of the chain to $\rho_+(J)$ at its right end. This prediction is compared to numerical simulation data in Fig. 3 for external rates $\alpha = \beta = 0.75$,

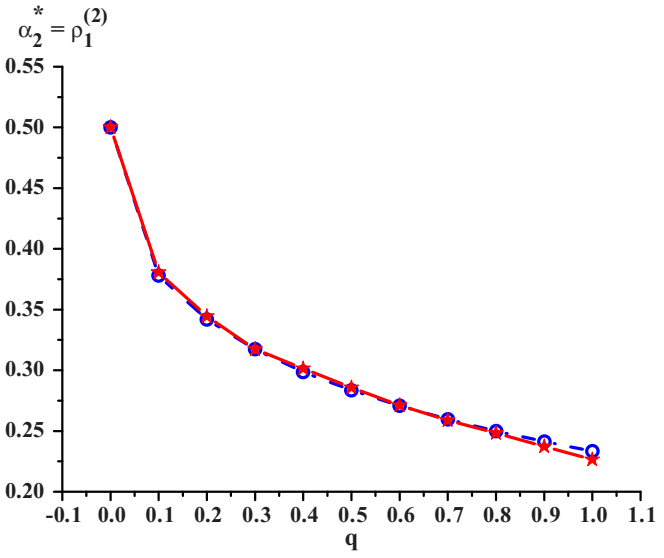


FIG. 2. (Color online) Comparison of the numerically evaluated $a_2^* = \rho_1^{(2)}$, shown by red stars, with the values of the appropriate root of the cubic equation (32), shown by blue circles, for different values of the rate $q$.

length of each segment $L = 400$, and $q = 0.5$. The data were averaged over 100 runs of length $2^{23}$ attempted moves each. One sees a good agreement between the theoretical prediction $\rho_1^{(2)} = \rho_-^{(2)} \simeq 0.282$ and the simulation result $\rho_1^{(2)} \simeq 0.286$. The agreement at the high-density end is also fairly good, between the theoretical prediction $\rho_{400}^{(2)} = \rho_+^{(2)} \simeq 0.718$ and the simulation result $\rho_{400}^{(2)} \simeq 0.701$.

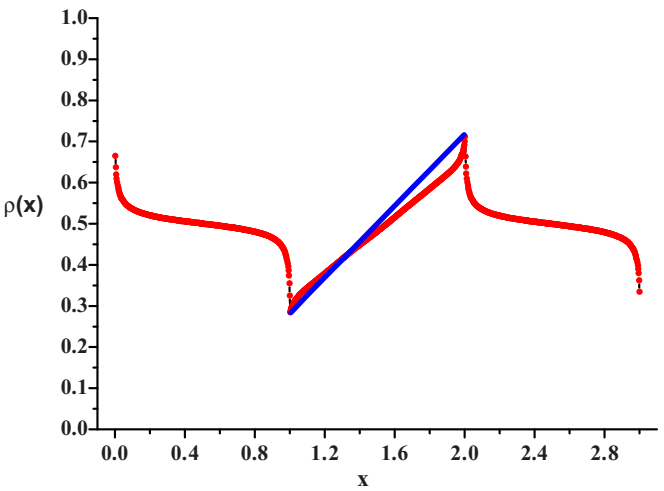


FIG. 3. (Color online) Local density profile at $\alpha = \beta = 0.75$ and $q = 0.5$ shown by red stars as a function of the normalized coordinate $x = i/L$, where $i = (s-1)L+1, (s-1)L+2, \ldots, sL$ labels the sites in the segment $s$, $s = 1,2,3$. The shape of the density profile in the first and third segments is typical for the maximum current phase, while that in the second segment closely resembles the linear dependence with the distance characteristic of the coexistence phase with a completely delocalized domain wall. The predictions of the domain wall theory are shown by a blue line.

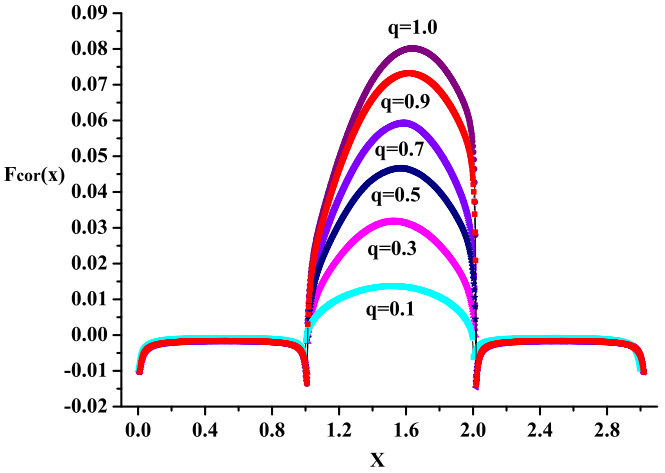


FIG. 4. (Color online) Position dependence of the nearest-neighbor correlations along the network at different values of $q$. The normalized coordinate $x = i/L$ is the same as in Fig. 3.

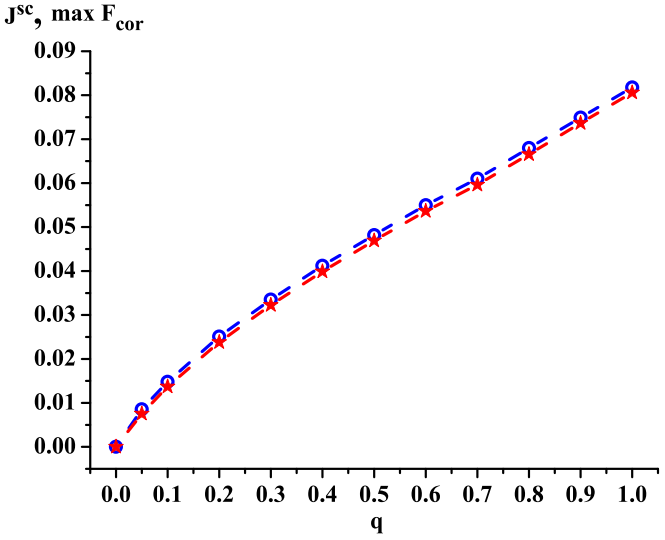


FIG. 5. (Color online) Comparison between the numerically estimated maximum value of the nearest-neighbor correlations in the second segment $\max_x F_{\rm cor}(x)$, shown by red stars connected with a red line, and the current $J^{\rm sc}$ through the shortcut, shown by blue circles connected with a blue line, at different values of the parameter $q$.

Another important prediction of the domain wall theory is the parabolic shape of the nearest-neighbor correlations

$$F_{\rm cor}(x) = \langle \tau_i^{(2)} \tau_{i+1}^{(2)} \rangle - \langle \tau_i^{(2)} \rangle \langle \tau_{i+1}^{(2)} \rangle$$

as a function of the normalized distance $x = i/L$. The simulation results for all $q$ show almost vanishing correlations in the bulk of the first and third segments and a parabolic-like shape in the second segment; see Fig. 4. The noticeable tilt of the "parabolas" to the right when $q \geqslant 0.7$ may be due to the different value of the correlations $G^{(s,s+1)}$ between the segments $s$ and $s+1$, $s = 1,2$. For example, we have numerically evaluated $G^{(1,2)} \simeq -0.0073$ at both $q = 0.3$ and $q = 1.0$, while $G^{(2,3)} \simeq -0.0023$ at $q = 0.3$ but $G^{(2,3)} \simeq 0.0095$ at $q = 1.0$. Theoretically, the maximum value of $F_{\rm cor}(x)$ is reached at the midpoint of the chain and equals

$$\max_x F_{\rm cor}(x) = \left[\rho_+^{(2)} - \rho_-^{(2)}\right]^2/4 = 1/4 - J^{(2)} = J^{\rm sc}. \quad (33)$$

The validity of this prediction of the domain wall theory is illustrated in Fig. 5. Remarkably, the value of $J^{\rm sc}$ determines also the endpoints of the linear profile,

$$\rho_{1,L}^{(2)} = 1/2 \mp \sqrt{J^{\rm sc}}. \quad (34)$$

We emphasize that Eqs. (33) and (34) are universal with respect to the shortcut nature. Thus, the main characteristics of the shunted section of a chain which is carrying maximum current depend only on the value of the current through the shortcut and do not depend on the structure of the latter.

## IV. DISCUSSION

In the framework of the effective rates approach [9] we reconsidered the simple model of a long open chain with zero-length shortcut in the bulk, suggested as "model A" in Ref. [13]. In contrast to those authors, we analytically solved the set of four equations for the four effective rates in the case when the network carries maximum current and the second (shunted) segment is either in a low- or in a high-density phase. We found out that in both cases the solution depends on one free parameter: the effective injection rate of the second segment in the former case and the effective ejection rate of the same segment in the latter case. In the space of the corresponding free parameter, the boundary of each phase obeys a cubic inequality with coefficients linearly depending the shortcut probability; see inequalities (16) and (23). At the common point of the closed domains, when the effective injection and ejection rates are equal, and less than $1/2$, the second segment can be found on the coexistence line. Here the values of the current and the local densities at the endpoints of the density profile are determined through Eqs. (24)–(26) by the positive solution, less than $1/2$, of the cubic equation (32).

Since the system is open, the low-density and high-density domains can be separated by a completely delocalized domain wall. Then the domain wall theory predicts linear spatial dependence of the local density profile and a parabolic one of the nearest-neighbor correlations in the shunted segment These predictions were confirmed by extensive computer simulations; see Figs. 3 and 4. Finally, Eqs. (33) and (34) establish that the endpoints of the linear density profile and the maximum of the parabolic nearest-neighbor correlations depend solely on the shortcut current, independently of the nature of the shortcut. This conclusion is supported by our results on chains with a section in the middle which consists of two equivalent parallel chains [9], when one of the parallel chains is considered as a "shortcut." In that case $J^{\rm sc} = J^{(2)} = 1/8$ and Eqs. (33) and (34) agree fairly well with the results shown in Figs. 8 and 9 in Ref. [9] see also the comparison between theoretical predictions and simulation results given in Eq. (67) there.

Results with somewhat better statistics for the local density profile in a network with segments of length $L_1 = L_2 = L_3 = 400$ and a shortcut realized by a chain of length $L^{\rm sc} = 100$ are shown in Fig. 6. The data are averaged over 100 independent runs of length $2^{23}$ attempts each. For the maximum of the

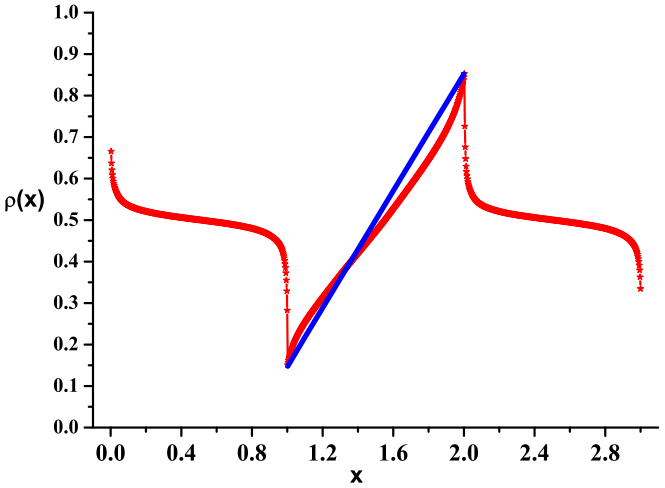


FIG. 6. (Color online) Local density profile at $\alpha = \beta = 0.75$ in a network with segments of length $L_1 = L_2 = L_3 = 400$ and a shortcut realized by a chain of length $L^{sc} = 100$ is shown by red stars. The predictions of the domain wall theory are shown by a blue line. The normalized coordinate $x$ is the same as in Fig. 3.

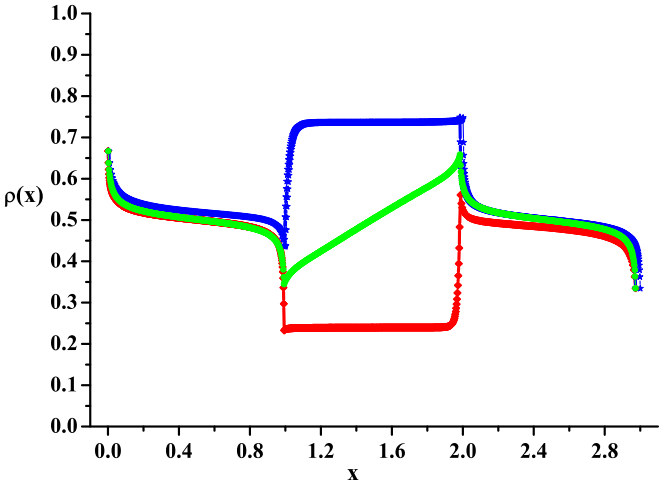


FIG. 7. (Color online) Numerical results for the local density profile $\rho(x)$ at $\alpha = \beta = 0.75$ in networks with different position of the shortcut: (a) For segments of length $L_1 = 200$, $L_2 = 400$, $L_3 = 600$, the profile in the second segment, shown in blue stars, is typical for a high-density phase; (b) for segments of length $L_1 = 600$, $L_2 = 400$, $L_3 = 200$, that profile, shown in red rotated squares, is typical for a low-density phase; (c) the case of equal length chains, $L_1 = L_2 = L_3 = 400$, corresponds to a coexistence phase in the second segment with a linear profile, shown in green disks, as predicted by the domain wall theory. The normalized coordinate $x$ is the same as in Fig. 3.

nearest-neighbor correlations we have now $\max_x F_{cor}(x) = 0.123$ to be compared to $J^{sc} = 0.125$.

In contrast to our study, the authors of Ref. [13] found it difficult to obtain analytical solutions for the set of effective rates for "model A" when the first and third segments are in the maximum current phase. Their computer simulations display only the $(\mathcal{M}, \mathcal{H}, \mathcal{M})$ phase structure of the network. However, in the cases when the first and third segments are both in the low-density or high-density phase, their results agree with ours.

We are not aware of any analytical study, within the effective rates approximation, of "model B" which involves two types of particles. It seems instructive to continue investigations in that direction.

Here it is worth noting that the presented theory neglects finite-size effects, since it uses results for the density profiles which are exact in the thermodynamic limit. Moreover, its validity is restricted to the extent to which correlations between different macroscopic segments can be neglected.

We have empirically established that the middle segment of the network is in a coexistence phase when its first and third segments are of equal length and the values of the injection and ejection rates at the external sites of the network are equal too, $\alpha = \beta > 1/2$. In our paper [12] we have found that if in a finite-size system a double-chain section is moved from the central position forward or backward, keeping constant the overall length of the network, the effective rates and of each of these chains change: from $\alpha_2^* \simeq \beta_2^*$ to $\alpha_2^* > \beta_2^*$ in the first case, or to $\alpha_2^* < \beta_2^*$ in the second one. Accordingly, the shape of the local density profiles changes from almost linear, typical for the coexistence phase ($\alpha_2^* \simeq \beta_2^*$), to one typical for the high- (low-) density phase when $\alpha_2^* > \beta_2^*$ ($\alpha_2^* < \beta_2^*$). A similar effect is observed in the present model too; see Fig. 7.

Summarizing, the most unexpected result is the model prediction that a shortcut in the bulk of a single lane, carrying a maximum stationary current, may cause traffic jams characteristic of a shock phase with a completely delocalized domain wall. The next unexpected result is the universal dependence of the main features of the shunted segment on the current through the shortcut.

## ACKNOWLEDGMENTS

N.B. gratefully acknowledges support from a grant of the Representative Plenipotentiary of Bulgaria to the Joint Institute for Nuclear Research in Dubna. A part of this work is based on research (N.P.) supported by the Research Chair in Mathematical Modelling and Methods in Bioengineering and Biosciences of the DST and NRF of South Africa.

[1] C. T. MacDonald, J. H. Gibbs, and A. C. Pipkin, Biopolymers **6**, 1 (1968).

[2] K. Nagel and M. Schreckenberg, J. Phys. I (France) **2**, 2221 (1992); D. Chowdhury, L. Santen, and A. Schadschneider, Phys. Rep. **329**, 199 (2000); D. Helbing, Rev. Mod. Phys. **73**, 1067 (2001).

[3] A. Parmeggiani, T. Franosch, and E. Frey, Phys. Rev. Lett. **90**, 086601 (2003); A. Roux, G. Capello, J. Cartaud, J. Prost, B. Goud, and P. Bassereau, Proc. Natl. Acad. Sci. USA **99**, 5394 (2002); G. Koster, M. VanDuijn, B. Hofs, and M. Dogterom, *ibid.* **100**, 15583 (2003); T. M. Nieuwenhuizen, S. Klumpp, and R. Lipowsky, Phys. Rev. E **69**, 061911 (2004);

C. Leduc, O. Campas, K. B. Zeldovich, A. Roux, P. Jolimaitre, L. Bourel-Bonnet, B. Goud, J.-F. Joanny, P. Bassereau, and J. Prost, Proc. Natl. Acad. Sci. USA **101**, 17096 (2004); C. Leduc, K. Padberg-Gehle, V. Varga, D. Helbing, S. Diez, and J. Howard, *ibid.* **109**, 6100 (2013); I. Neri, N. Kern, and A. Parmeggiani, Phys. Rev. Lett. **110**, 098102 (2013).

[4] J. Krug and H. Spohn, Phys. Rev. A **38**, 4271 (1988); J. Krug, P. Meakin, and T. Halpin-Healy, *ibid.* **45**, 638 (1992); T. Sasamoto, J. Phys. A **38**, L549 (2005).

[5] T. Chou and D. Lohse, Phys. Rev. Lett. **82**, 3552 (1999); Q.-H. Wei, C. Bechinger, and P. Leiderer, Science **287**, 625 (2000); A. B. Kolomeisky, Phys. Rev. Lett. **98**, 048105 (2007).

[6] T. Reichenbach, E. Frey, and T. Franosch, New J. Phys. **9**, 159 (2007).

[7] T. Huisinga, R. Barlovic, W. Knopse, A. Schadschneider, and M. Schreckenberg, Physica A **294**, 249 (2001).

[8] T. Karzig and F. von Oppen, Phys. Rev. B **81**, 045317 (2010).

[9] J. Brankov, N. Pesheva, and N. Bunzarova, Phys. Rev. E **69**, 066128 (2004).

[10] E. Pronina and A. B. Kolomeisky, J. Stat. Mech. Theor. Exp. 07 (2005) P07010.

[11] P. Pierobon, M. Mobilia, R. Kouyos, and E. Frey, Phys. Rev. E **74**, 031906 (2006); Z.-P. Cai, Y.-M. Yang, R. Jiang, M.-B. Hu, Q.-S. Wu, and Y.-H. Wu, J. Stat. Mech. Theor. Exp. 07 (2008) P07016; B. Embley, A. Parmeggiani, and N. Kern, J. Phys.: Condens. Matter **20**, 295213 (2008); Z.-P. Cai, Y.-M. Yuan, R. Jiang, K. Nishinary, and Q.-S. Wu, J. Stat. Mech. Theor. Exp. 02 (2009) P02050; X. Wang, R. Jiang, K. Nishinary, M.-B. Hu, and Q.-S. Wu, Int. J. Mod. Phys. C **20**, 967 (2009); X. Wang, R. Jiang, M.-B. Hu, K. Nishinary, M.-B. Hu, and Q.-S. Wu, *ibid.* **20**, 1999 (2009); B. Embley, A. Parmeggiani, and N. Kern, Phys. Rev. E **80**, 041128 (2009); H.-F. Du, Y.-M. Yuan, M.-B. Hu, R. Wang, R. Jiang, and Q.-S. Wu, J. Stat. Mech. Theor. Exp. 03 (2010) P03014; I. Neri, N. Kern, and A. Parmeggiani, Phys. Rev. Lett. **107**, 068702 (2011); X. Song, L. Ming-Zhe, W. Jian-Jun, and W. Hua, Chin. Phys. B **20**, 060509 (2011); S. Xia, L. Tang, and H. Wang, Cent. Eur. J. Phys. **9**, 1077 (2011); C. Appert-Rolland, J. Cividini, and H. J. Hilhorst, J. Stat. Mech. Theor. Exp. 10 (2011) P10014; R. Chatterjee, A. K. Chandra, and A. Basu, Phys. Rev. E **87**, 032157 (2013); A. Raguin, A. Parmeggiani, and N. Kern, *ibid.* **88**, 042104 (2013).

[12] N. C. Pesheva and J. G. Brankov, Phys. Rev. E **87**, 062116 (2013).

[13] Y.-M. Yuan, R. Jiang, R. Wang, M.-B. Hu, and Q.-S. Wu, J. Phys. A **40**, 12351 (2007).

[14] B. Derrida, E. Domany, and D. Mukamel, J. Stat. Phys. **69**, 667 (1992); B. Derrida, M. R. Evans, V. Hakim, and V. Pasquier, J. Phys. A: Math. Gen. **26**, 1493 (1993).

[15] A. B. Kolomeisky, G. M. Schüutz, E. B. Kolomeisky, and J. P. Straley, J. Phys. A **31**, 6911 (1998); L. Santen and C. Appert, J. Stat. Phys. **106**, 187 (2002).